

Biarticular Muscles Improve the Stability of a Neuromechanical Model of the Rat Hindlimb

Kaiyu Deng¹(⊠), Alexander J. Hunt², Hillel J. Chiel¹, and Roger D. Quinn¹

 Case Western Reserve University, Cleveland, OH, USA kxd194@case.edu
 Portland State University, Portland, OR, USA

Abstract. This study introduces a novel neuromechanical model of rat hindlimbs with biarticular muscles producing walking movements without ground contact. The design of the control network is informed by the findings from our previous investigations into two-layer central pattern generators (CPGs). Specifically, we examined one plausible synthetic nervous system (SNS) designed to actuate 3 biarticular muscles, including the Biceps femoris posterior (BFP) and Rectus femoris (RF), both of which provide torque about the hip and knee joints. We conducted multiple perturbation tests on the simulation model to investigate the contribution of these two biarticular muscles in stabilizing perturbed hindlimb walking movements. We tested the BFP and RF muscles under three conditions: active, only passive tension, and fully disabled. Our results show that when these two biarticular muscles were active, they not only reduced the impact of external torques, but also facilitated rapid coordination of motion phases. As a result, the hindlimb model with biarticular muscles demonstrated faster recovery compared to our previous monoarticular muscle model.

 $\textbf{Keywords:} \ \ \text{Rat} \cdot \text{Biarticular Muscles} \cdot \text{Synthetic Nervous System} \cdot \text{Stabilization Analysis}$

1 Introduction

Recent technological advancements have led to the development of legged robots that exhibit greater agility and stability, even when encountering unexpected perturbations during various locomotor tasks [1–4]. Despite these impressive developments, there is a growing interest in the remarkable ability of animals to effectively solve low-level joint/gait coordination problems while adapting to changes in their environment. This highlights the importance of studying natural mechanisms and suggests that researchers can gain valuable insights into the development of more advanced bio-inspired robots and prosthetic devices.

Despite the existence of promising bio-inspired robots [5–10] and artificial neural controllers [11–15], our current understanding of the mechanisms behind dynamic and robust walking is still insufficient for the development of robots that mimic mammalian

locomotion. Although the strategies and neural systems responsible for mammalian locomotion patterns are not yet fully understood, cat locomotion studies using split-belt treadmills suggest that the spinal cord and its associated peripheral nervous system are pivotal in generating and adapting these patterns [16–18]. This is consistent with T.G. Brown's finding that the cat spinal cord can generate a locomotor rhythm in the absence of input from higher centers and afferent feedback [19].

Subsequent investigations confirmed Brown's findings and led to the development of the widely accepted concept of central pattern generators (CPGs). These are neural circuits located within the central nervous systems of invertebrates and vertebrates that can generate rhythmic, coordinated movements such as swimming [20], walking [21–23], heartbeat [24], breathing and gasping [25]. The "half-center" model [21] is a widely used model of the spinal CPG that produces rhythmic alternating activity of flexor and extensor motoneurons during locomotion.

However, the presence of "non-resetting deletions" [26], observed in the movement of decerebrate cats cannot be explained by a simple "half-center" structure. These "non-resetting deletions" refer to instances where motoneuron activities are absent for a few cycles, but then reappear without a phase shift. To address this issue, Rybak's group proposed a computational model of the two-layer CPG [27], which allows for separate control of walking rhythm timing and motoneuron activity pattern during locomotion.

Our previous work incorporated a two-layer CPG into a neuromechanical model of rat hindlimbs [15], which successfully reproduced repetitive forward walking and "non-resetting deletions". However, this neuromechanical model was limited by its simplistic musculoskeletal configuration with pairs of antagonist muscles at each joint. As a result, the stability investigations from this model were potentially incomplete. To address this issue, we have expanded the musculoskeletal configuration to include biarticular muscles in a simplified model [28] and a full-muscle model [29]. Our current goal is to investigate how biarticular muscles could contribute to the stabilization of the simulation model during walking. Specifically, we explore how biarticular muscles linking hip and knee joint are actuated with a plausible neural configuration that utilizes the preferred CPG parameters reported in a previous work by our group [30].

2 Methods

To simulate the rat hindlimb walking with biarticular muscles, we used Animatlab [31], a simulation software that allows for the creation of synthetic nervous systems (SNSs) and actuation of biomechanical bodies with proprioceptive feedback. The simulations were conducted in the Vortex physics engine (CM Labs, Montreal, Quebec), which is integrated into Animatlab and provides realistic physical simulations.

2.1 Biomechanical Modeling

The biomechanical model of the rat hindlimb (shown in Fig. 1A) and muscle parameter values are consistent with our previous model [28]. As in the previous model, the hindlimb is constrained to move in the sagittal plane and is actuated by the eight most prominent muscles used in forward locomotion. The hindlimb model consists of five

monoarticular muscles, including Iliopsoas (IP) and Biceps femoris anterior (BFA), which actuate the hip joint; grouped Vastii (VA), which actuates the knee joint; and Soleus (SO) and Tibialis anterior (TA), which actuate the ankle joint. The model also includes three biarticular muscles shown in red font, including Biceps femoris posterior (BFP) and Rectus femoris (RF), which link the hip and knee joint and are the primary focus of investigation in this study; while Gastrocnemii (GA) spans the knee and ankle joint.

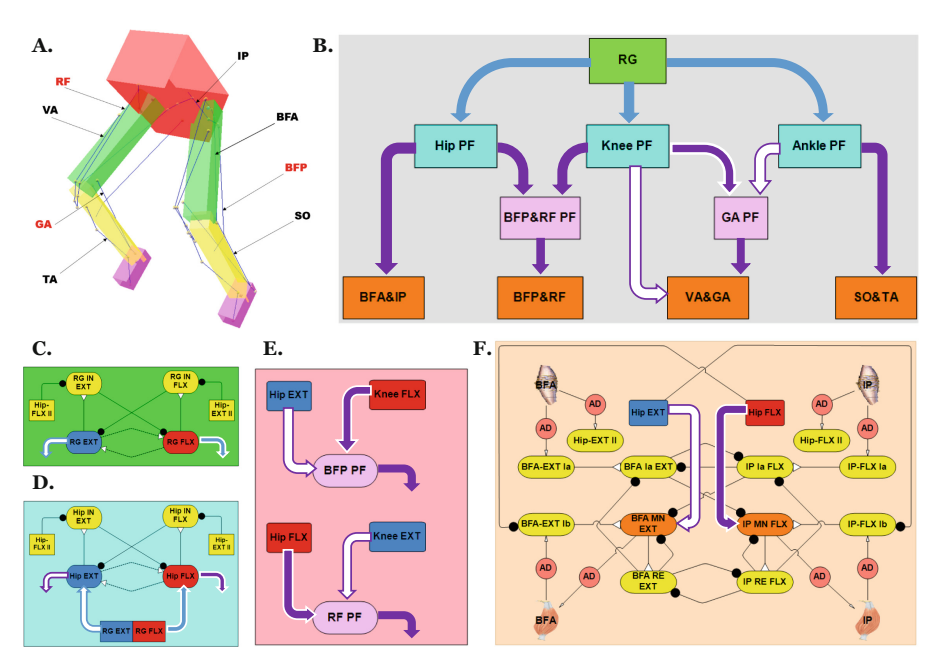


Fig. 1. Neuromechanical model of rat hindlimbs. (A) Biomechanical model of the rat hindlimbs from our previous work [28], muscle labeled in red font are biarticular muscles. (B) Schematic of the general neural control network for a single rat hindlimb. (C) General rhythm generator configuration. (D) Pattern formation network for the hip joint. (E) Intermediate integration layer for the BFP and RF muscles. GA PF similarly combines Ankle EXT and Knee FLX signals. (F) Sensory-motor network for the hip monoarticular muscle pair (BFA & IP). Identical network designs are used for BFP and RF, VA and GA, and SO and TA. IP: Iliopsoas; BFA: Biceps femoris anterior; BFP: Biceps femoris posterior; SO: Soleus; RF: Rectus femoris; VA: Vastii; GA: Gastrocnemii; TA: Tibialis anterior. RG: Rhythm generator; PF: Pattern formation; MN: motoneuron; IN: Interneuron; EXT: Extensor; FLX: Flexor; RE: Renshaw cell; AD: Adaptor. Color codes are used to distinguish between neurons and connections. Extensor oscillators are colored blue, while flexor oscillators are colored red. Motoneurons are colored brown, interneurons are colored yellow, and pink indicates intermediate pattern formation interneurons for biarticular muscles. Flexor signals are indicated by arrows with solid fill and white outline, while extensor signals are represented by arrows with a white fill and solid outline. Arrows with both solid fill and outline indicate that all signals are conducted to the next region.

AnimatLab uses a basic linear Hill muscle model from Shadmehr's work [32, 33] to generate force and it is illustrated in Fig. 2 below.

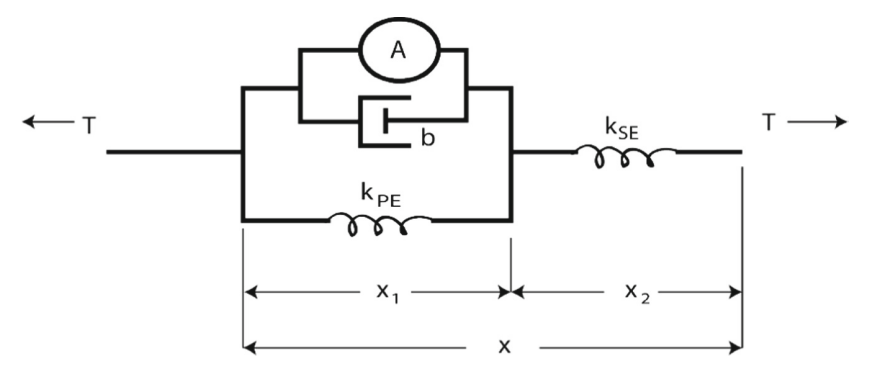


Fig. 2. AnimatLab Muscle Model. Adapted from Shadmehr's work [32, 33].

The muscle model is a spring-damper system with user pre-defined length-tension and stimulus-tension relationships. Tension, T, developed in the muscle is determined by the following equation:

$$\frac{dT}{dt} = \frac{k_{se}}{b} \left(k_{pe} \Delta x + b\dot{x} - \left(1 + \frac{k_{pe}}{k_{se}} \right) \cdot T + A \right)$$

where Δx is the muscle length minus the resting length (if negative, $\Delta x = 0$), \dot{x} is the muscle contraction velocity, k_{se} is the series elastic stiffness and k_{pe} is the parallel elastic stiffness, b is the linear muscle damping, and A represents the activation level of the muscle described by:

$$A = A_m * A_l$$

where A_m is the stimulus-tension factor:

$$A_m = \frac{F_{max}}{1 + e^{C(V_0 - V)} + B}$$

where F_{max} is the maximum muscle force, C describes the slope of the sigmoid, V is the membrane voltage of the motor neuron, and V_0 and B describe the V and F offsets of the sigmoid. A_l is the length-tension factor described as:

$$A_l = 1 - \frac{(l - l_{rest})^2}{l_{width}^2}$$

where l_{rest} describes the length at which the muscle can provide the most force and l_{width} describes the length from l_{rest} at which the muscle can provide no force. Details of the muscle parameter design can be found in Deng et al. [28].

The afferent feedback used in this paper are simplified representations of types Ia, Ib, and II (shown in Fig. 1) in mammalian systems modeled by Animatlab. Ia feedback is sensitive to muscle velocity \dot{x} and total muscle length x, Ib feedback is dependent on the muscle tension T, and II feedback is dependent on length of parallel elastic element x_1 . Ia and Ib feedback are synapsed onto correspondent motoneuron pools as shown in Fig. 1F. Type II feedback from the hip monoarticular muscles (namely BFA and IP) were applied directly to the rhythm generator (Fig. 1C) and the pattern formation networks (Fig. 1D) to coordinate the extensor-flexor timing.

2.2 Neural Modeling

The precise mechanisms underlying control of biarticular muscles are not yet fully understood. In light of this incomplete understanding, we have developed a hypothesis for the neural architecture involved in biarticular muscle control, which is depicted in Fig. 1B. The proposed SNS shares similarities with our previously developed two-layer CPG network, but features an additional intermediate layer between the CPG network and the sensory-motor network. This layer processes pattern signals from related joints and integrates them to produce more precise and accurate patterns for biarticular muscle control.

In Fig. 1, panels B through F, we employed a color scheme to differentiate between neurons and connections. Specifically, the extensor oscillators are denoted by the color blue, while flexor oscillators are represented by the color red. In addition, motoneurons are depicted in brown, interneurons in yellow, and the intermediate pattern formation interneurons for biarticular muscles in pink. To further differentiate between flexor and extensor signals, arrows with a solid fill and white outline are used to indicate flexor signals, while arrows with a white fill and solid outline depict extensor signals. Arrows that feature both solid fill and outline indicate that all signals are transmitted to the following region.

In this study, each neuron node depicted in Fig. 1 represents the average activity of a population of spiking neurons, and functions as a leaky integrator [34]. All neurons are modeled as conductance-based, non-spiking compartments; action potentials were neglected in the model to increase computational efficiency and reduce runtime [35]. This simplification allows us to focus on how signals are transmitted through synapses and how groups of neurons contribute to network behaviors.

The membrane voltage of a neuron node, V, may be seen as a proxy for the spiking frequency of a spiking neuron. V varies according to the differential equation:

$$C_m \frac{dV}{dt} = G_m(E_{rest} - V) + \sum_{i=1}^n G_{s,i} \cdot (E_{s,i} - V)$$
$$+ I_{app} + G_{NaP}(E_{NaP} - V) \cdot m_{\infty} \cdot h$$

where I_{app} is external stimulus, E_{rest} is the resting potential of the neuron, t is the time variable and E stands for a constant reference voltage (i.e. reversal potential). C_m and G_m are the capacitance and conductance of the cell membrane, respectively. The conductance, $G_{s,i}$ is a threshold linear function of the i^{th} incoming (i.e. presynaptic)

neuron's voltage. Synapses communicate via piecewise-linear functions described as:

$$G_{s,i} = g_{s,i} \cdot min\left(max\left(\frac{V_{pre} - E_{lo}}{E_{hi} - E_{lo}}, 0\right), 1\right)$$

where $g_{s,i}$, E_{lo} , and E_{hi} are constants representing the i^{th} synapse's maximum conductance, its lower threshold, and its upper threshold, respectively. $G_{NaP}(E_{NaP} - V)$ is a persistent sodium current present in the oscillator neurons with voltage-dependent channel activation and deactivation described by m and h:

$$\frac{dh}{dt} = \frac{h_{\infty}(V) - h}{\tau_h(V)}, \quad \tau_h(V) = \tau_h \cdot h_{\infty}(V) \cdot \sqrt{A_h \cdot \exp(-S_h(V - E_h))}$$

For each instance of ion use, m_{∞} and h_{∞} values were adjusted to match with other CPG models developed in the field [36, 37]. Both m_{∞} and h_{∞} are sigmoidal function described below:

$$z_{\infty} = \frac{1}{1 + A_z \cdot exp(-S_z(V - E_z))}$$

where z represents either m or h, ,, and A (factor), S (slope) and E (reversal potential) are constant parameters, specific to m or h.

The oscillators in the PF incorporate the same persistent sodium current as the RG ones, which means that they can produce the same rhythm as RG neurons. In our prior analysis of the two-layer CPG, we primarily investigated the perturbation response of a single joint (the hip joint) [30]. In this paper, we will investigate how the two-layer CPG performs in controlling multiple joints while responding to different disturbances. Our previous investigations [30] showed how different parameters affect coordination between the RG and PF layers and provides the basis for the parameters chosen in this work and reported in the Appendix (Tables 1 and 2). The maximum conductance value (g_c) between the RG and PF, are as follows: 0.1 μ S for the hip joint, 0.05 μ S for the knee joint, and 0.02 μ S for the ankle joint. This allocation of maximum conductance followed the report from our previous investigations of the two-layer CPG, which suggested that more distal segments require greater flexibility in responding to perturbations.

Figure 3 provides a graphical representation of the activation of neurons in a twolayer CPG that controls multiple joints in the hindlimb under unperturbed conditions. The rhythm generator sets the oscillatory frequency of the joint movements, whereas the pattern formation network modulates the amplitude of the oscillations and the phase relationship between the joints.

In particular, each joint's CPG oscillates at a consistent frequency (time for one step cycle is around $0.59 \, \mathrm{s}$), which is regulated by the rhythm generator. However, the pattern formation network of each joint exhibits a distinct phase timing (i.e. when compared to RG) that is unique to that joint. The hip joint exhibits a 5.74% phase delay, while the knee advances 6.35% and ankle advances 8.32% in phase. This is consistent with our previous report on g_c : The connection strength results in a trade-off between phase-locking potentials and the amount of phase difference that can exist between the two layers.

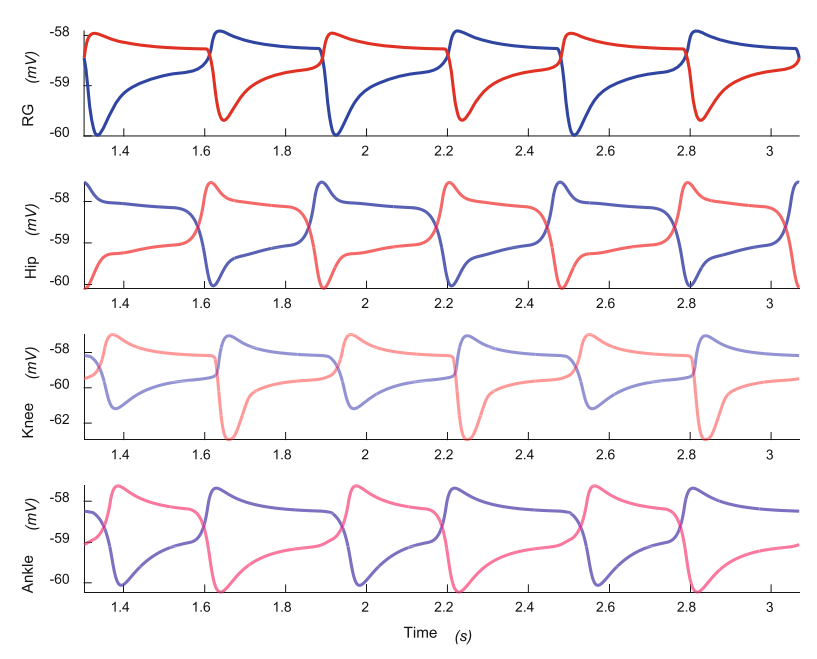


Fig. 3. Neuron activity for the two-layer CPG controlling multiple joints. The rhythm generator controls the overall timing of the network. Each joint pattern formation network exhibit different phase timings, all while maintaining the same oscillation frequency. The hip joint exhibits a 5.74% phase delay, while the knee joint advances 6.35% and the ankle joint advances 8.32% in phase. However, the period for one step for all these joints persists at 0.59 s per cycle. The blue lines represent the membrane voltage for extensor neurons, and the red lines stand for flexor neuron voltages.

3 Results

We started by manually adjusting the connection strengths and feedback weights of the hindlimb model, fine-tuning it until it was capable of sustaining its own weight while achieving repetitive forward walking with biarticular muscles. To further evaluate the performance of the model, we then suspended the pelvis of the model in the air to allow the model to perform repetitive movements without ground contact. We did this because in later experiments, we disabled the biarticular femoral muscles (BFP and RF) which are important for supporting the body's weight during movement.

We first perturbed the simulation model by introducing external currents to different layers of the two-layer CPG and analyzed the model's response. Subsequently, we applied torque to the hindlimb model's right femur under three different circumstances: with the BFP and RF muscles active and functioning normally, with only passive tension in the BFP and RF (by disabling the motoneuron projection), and with the BFP and RF muscles fully disabled, rendering the model monoarticular at the hip joint.

3.1 CPG Perturbation Test

Applying an external stimulus current with a magnitude of 2 nA to the flexor neuron of the rhythm generator from 2 s to 2.1 s (orange area in Fig. 4) resulted in a rapid short step, followed by a 15.44% phase–delayed step cycle after the perturbation, and subsequent step cycles exhibited a 15% phase delay.

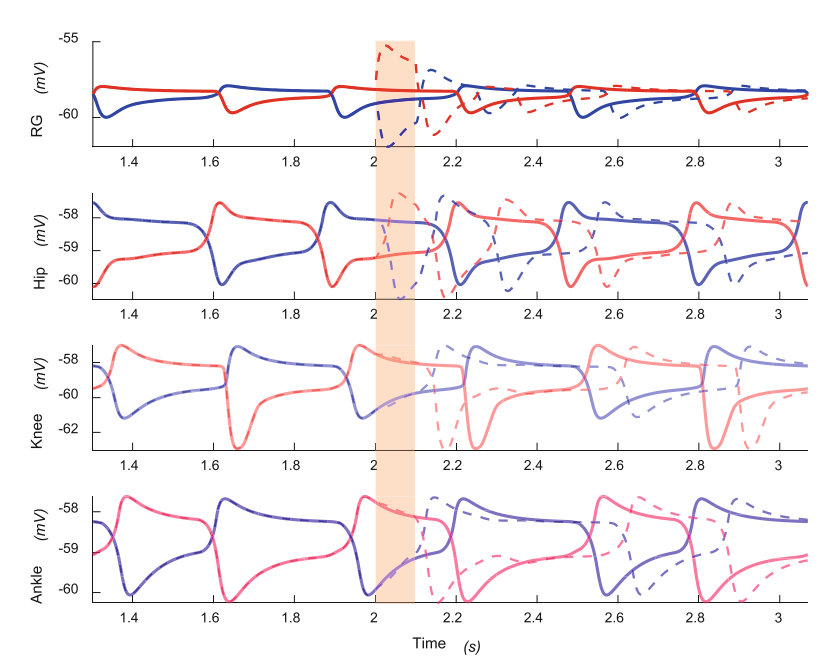


Fig. 4. Neuron activity when the RG layer is perturbed. An external stimulus with a magnitude of 2 nA is applied to the flexor neuron of the rhythm generator, starting at 2 s and ending at 2.1 s (orange area). The external stimulus causes a rapid short step with phase delay of 15.44% for the next step cycle after injection, followed by 15% phase delays for the subsequent step cycles. Strong connections ($g_c = 0.1uS$) ensure that the hip strictly follows the signal patterns from the rhythm generator, while weak connections ($g_c = 0.05uS$ for the knee and $g_c = 0.02uS$ for the ankle) result in a less perturbed phase (with a skipped step) of the knee and ankle joints. However, the knee and ankle still follow the phase timing from the rhythm generator after the perturbation. Blue lines represent the membrane voltage for extensor neurons, and the red lines stand for flexor neuron voltages. The solid lines represent the nominal activation of neurons in the two-layer CPG, while the dashed lines indicate the neuron activations during perturbed motion.

And the resulting patterns depicted in Fig. 4 demonstrate that a strong connection enables the hip joint to closely adhere to the signal patterns from the rhythm generator (5.74% phase delays). In contrast, weak connections result in a less disturbed phase (with a skipped step) of the knee and ankle joints during the disturbance. In either case, after injection, the neuron activity from the knee and ankle remains synchronized with the phase timing from the rhythm generator (i.e. the knee advances 6.35% and ankle advances 8.32% in phase).

Applying a 2 nA external current to the flexor neuron of the knee pattern formation network from 2 s to 2.1 s (orange area in Fig. 5) produces results that contradict previous experiments involving only antagonistic muscle pairs.

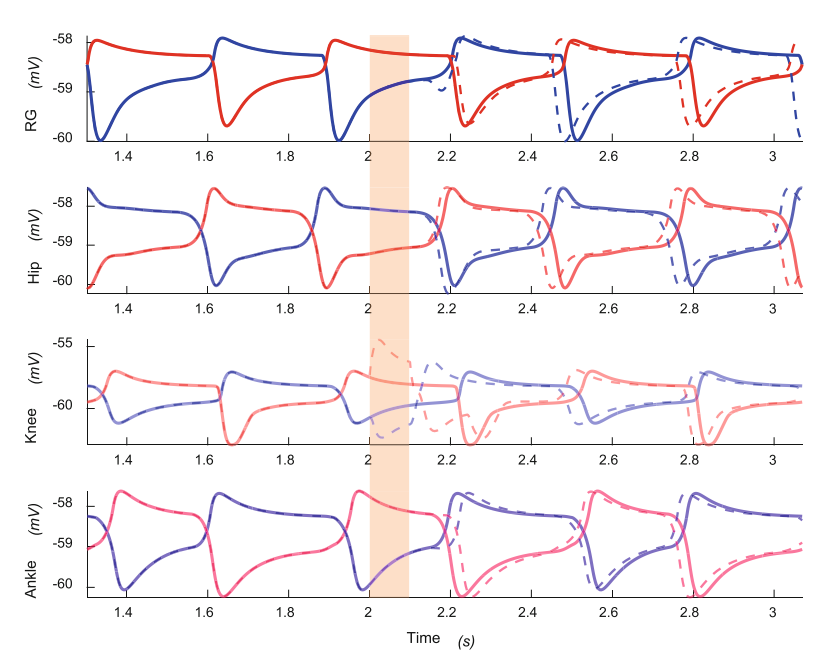


Fig. 5. Neuron activity when the knee joint is perturbed. An external stimulus with a magnitude of 2 nA is applied to the flexor neuron of the knee pattern formation network, starting at 2 s and ending at 2.1 s (orange area). This perturbation of the knee joint leads to a phase shift in all the joints. To clarify, the initial step after injection involves advancing the rhythm generator by 5%, the hip joint by 5.3%, the knee joint by 6.7%, and the ankle joint by 3%. Then, in the subsequent steps, all joints are advanced by 5.2% in response to the phase-advanced rhythm generator signal. The membrane voltage of extensor neurons is indicated by blue lines, while that of flexor neurons is represented by red lines. The solid lines represent the nominal activation of neurons in the two-layer CPG, while the dashed lines indicate the neuron activations during perturbed motion.

In our prior research on the rat hindlimb simulation model with antagonist muscles, we found that perturbing the pattern formation network of a single joint did not affect the neuron activations of the rhythm generator or the motion of other joints. However, in this current study, we observed a phase shift in other joints when an excitatory stimulus is applied to the knee flexor neuron of the pattern formation network. Specifically, after injection, the first step cycle is advanced by 5% for the rhythm generator, 5.3% for the hip joint, 6.7% for the knee joint and 3% for the ankle joint. Subsequently, following the signal from the phase-advanced rhythm generator, all the joints are advanced by 5.2% in the following steps.

3.2 Joint Torque Perturbation Test

Figure 6 presents neural activity in the pattern formation network for all muscles during air-walking. The activation pattern for the monoarticular pairs in the hip joint (BFA and IP, color-coded as blue and red which stand for extension and flexion neuron voltage), respectively, generally follows the signal pattern depicted in Fig. 3. The same applies to the monoarticular pairs in the ankle joint (TA and SO). The same applies to the monoarticular muscles pairs (TA and SO) in the ankle joint. Since these muscles actuate only a single joint, they require a more straightforward signal pattern to execute their respective movements. In contrast, the biarticular muscles BFP (present in cyan line), RF (present in magenta line), and GA (present in pink line) integrate patterned signals from multiple joint networks, necessitating more complex signaling. As a result, these muscles exhibit a more intricate activation pattern than monoarticular muscles, which, in turn, generates a complex motion to control movement across multiple joints.

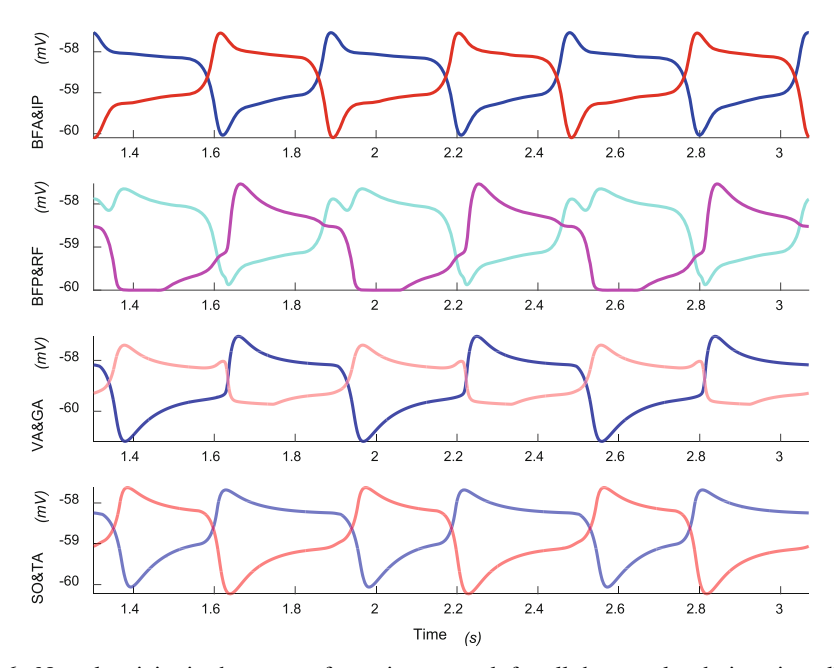


Fig. 6. Neural activity in the pattern formation network for all the muscles during air-walking. The monoarticular hip muscles BFA and IP, ankle muscles TA and SO generally follow the signal activation pattern presented in the Fig. 3, whereas the biarticular muscles BFP, RF, and GA integrate signal patterns from the actuated joints. Blue lines represent the membrane voltage for extensor neurons, and the red lines represent the flexor neuron voltages. The cyan line shows the activation for BFP, magenta presents the membrane voltage for RF, and the pink line depicts the GA.

When an external torque of 0.1 Nm is applied to the right femur in the simulation, the response of the biarticular muscles model under three different conditions during air-walking can be distinguished. As can be seen in Fig. 7, the magnitude of the phase changes due to the external torque is significantly less in the biarticular muscle models, regardless of whether there is active tension on the muscle or not. Thus, we conclude that biarticular muscles can reduce the impact of external perturbations. However, this reduction in perturbation also influences the motion of other joints, such as the knee and ankle.

Comparison of nominal and perturbed motions of the leg reveals that active BFA and RF muscles result in faster restoration when compared to model in which they are disabled. Interestingly, it was found that the biarticular muscle model with only passive tension was unable to return to its original step timing after the perturbation ended.

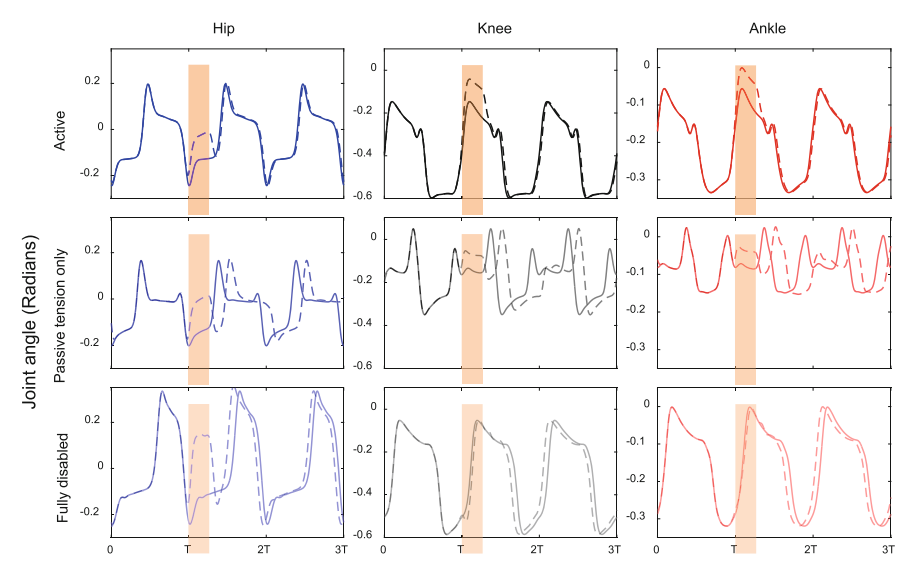


Fig. 7. Nominal (solid lines) and perturbed (dashed lines) joint motion for the biarticular muscles model under three different conditions: when the BFP and RF muscles are fully active (first row); when there is only passive tension on the BFP and RF muscles (second row); and when the BFP and RF muscles are fully disabled (third row). The joint motion profiles are depicted using blue lines for hip joint motion (orange areas shows when the external torques are applied), black lines represent knee motion, and red lines stand for ankle motion. The perturbation is an external torque with magnitude — 0.1 Nm applied to the right femur, starting at the beginning of the second stride and lasting for 30 percent of the stride period. During the perturbed motion, the full activation of the BFA and RF muscles results in better stability when compared to the monoarticular hip joint condition, as it enables faster and better recovery to the original step timing.

4 Discussion

In this work, we present a neuromechanical model of a rat hindlimb with biarticular muscles. We expanded on our previous study of biarticular muscle models [28] by examining the neural control of this model. In other previous work, we conducted an in-depth investigation of the two-layer CPG [30] and gained a better understanding of the design of these neural controllers. In this work, we integrated our prior findings to design a hypothesized SNS that actuates the biarticular muscles BFP and RF muscles connecting the hip and knee joints, and the GA muscle spanning the knee and ankle joint.

Biarticular muscles play an important role in locomotion. Previous research by Markin's group [38] and Shevtsova et al. [39] has proposed how biarticular muscles are controlled. Specifically, they suggest that the BFP and RF muscles have their own individual pattern formation networks. This enables more precise control of these muscles, but complicates the design of the SNS, and may require additional animal data to help tune the parameters in these individual pattern formation networks. Similarly, our hypothesized neural architecture comprises multiple components that collectively govern the timing and coordination of movement between the joints. Specifically, the rhythm generator plays a critical role in regulating the overall timing of steps, adjusting the timing of movement phases in each individual joint. The pattern formation networks for hindlimb joints receive input from the rhythm generator and distribute signals to the corresponding muscles and intermediate layers, which is necessary for coordinating the movements of the biarticular muscles. Notably, a difference in our network is that the muscles are organized into reciprocal synergist pairs and receive signal projections from joint level pattern formation networks.

In the CPG perturbation test, we found that the rhythm generator plays a crucial role in controlling the overall timing of the hindlimbs. Specifically, each pattern formation network of the joints displays distinct phase timings that are sensitive to perturbations applied at the rhythm generator layer. Strong connections between the rhythm generator and the hip joint enable the hip joint to closely adhere to the RG step timing during perturbations, while weaker connections lead to less disturbed phase timings in the knee and ankle joint. Importantly, the results observed in this study differ from those reported in previous works for monoarticular actuation. Specifically, we found that disrupting the knee's pattern formation network resulted in changes in motion at all the joints. Specifically, changes in knee kinematics affected the intermuscular coordination between the hip and knee joint, resulting in a cascade of effects. Changes in knee joint motion affected both the hip joint's motion and the phase of the rhythm generator. As the rhythm generator's phase shifts, the direct connection between the ankle and the rhythm generator causes the ankle phase to become correlated with the RG timing. These findings support our previous analysis of the two-layer CPG and confirm our expectations regarding the perturbation response of the system.

Based on the air-walking perturbation test simulation results, we discovered that biarticular muscles can significantly reduce the impact of external torque. This is evidenced by the smaller phase changes observed in the fully active biarticular muscle models compared to the monoarticular muscle models. However, this reduction in perturbation also influences the motion of other joints due to the multi-joint linkage through biarticular muscles. Additionally, our analysis revealed that activating the BFA and RF muscles resulted in faster restoration after the perturbation compared to the model with the biarticular muscles disabled. Interestingly, the biarticular muscle model with only passive tension on the muscle was unable to revert back to its original step timing after the perturbation ended, likely due to the considerable magnitude of passive tension as reported in our previous work [28]. A possible explanation for this is that the passive tension in the biarticular muscles acts as a large damper in the absence of active tension. This dampening effect reduces the impact of external torques and minimizes internal adjustments.

There are some limitations in our work that must be carefully considered. For instance, the muscle model utilized in AnimatLab does not employ a hyperbolic force-velocity relationship for the contractile element. It is possible that different muscle models may have an effect on the quantitative results, though we anticipate the qualitative results will remain the same. Furthermore, the joint angle ranges differ significantly between the three different situations in the air-walking perturbation test. As the models being compared are not optimally tuned, we can only conclude that the normal active biarticular muscle is less affected by external torque and exhibits faster restoration after perturbation, which provides more stability compared to the fully disabled model. It is still unclear if all these results will remain the same when each model is tuned for ground walking and the perturbations are applied in a more realistic environment. Indeed, previous results from our work indicate that all differences seen in neural perturbation and air-walking tests may functionally result in little to no difference when applied to ground walking [30].

While this work has shed light on the functional role of biarticular muscles in stabilizing perturbed locomotion, there are several limitations stemming from the lack of detailed rat locomotion and EMG data. However, these limitations do not diminish the value of our findings, which offer important insights into this complex phenomenon and provide guidelines for designing a neural controller for a biomechanical model with biarticular muscles. Moving forward, future research should investigate the impact of different SNS designs and noise on the stability of the model, and should also compare the results with neural controllers hypothesized by researchers in parallel studies. Also, a more in-depth analysis investigating perturbations with different amplitude, timing and directions is necessary to support our conclusion on a more general basis. Overall, this work highlights the significance of biarticular muscles in stabilizing the rat hindlimbs during perturbed locomotion, and the broader implications of our findings for understanding animal locomotion.

Acknowledgements. This work was supported by grants from the NSF DBI 2015317 as part of the NSF/CIHR/DFG/FRQ/UKRIMRC Next Generation Networks for the Neuroscience Program.

Appendix

List of Acronyms

CPG Central pattern generator

SNS Synthetic nervous system

BFP Biceps femoris posterior

RF Rectus femoris

GA Gastrocnemii

IP Iliopsoas

BPF Biceps femoris anterior

VA Vastii

SO Soleus

TA Tibialis anterior

RG Rhythm generator

PF Pattern formation

MN Motoneuron

IN Interneuron

RE Renshaw cell

EXT Extensor

FLX Flexor

AD Adaptor

Table 1. Neural parameters

Neuron	$C_m(nF)$	$G_m(\mu S)$	E_r (mV)	$G_{Na}(\mu S)$	A_h	S_h	E_h (mV)			Sm	E_m (mV)	τ_m (ms)
RG	5	1	-60	1.5	0.5	-0.6	-60	350	1	0.2	-40	2
PF	5	1	-60	1.5	0.5	-0.6	-60	350	1	0.2	-40	2
MN	5	1	-100	0	_	_	_	_	_	-	_	_
IN	5	1	-60	0	_	_	_	_	_	_	_	_

Synapse	g (μS)	E_s (mV)	E_{lo} (mV)	E_{hi} (mV)
DC to IN			-60	-40
RG to IN	2	-40		
IN to RG	2	-70	-60	-40
Between RG	0.01	-40	-60	-40
PF to IN	2	-40	-60	-40
IN to PF	1.61	-70	-60	-40
PF to MN	/→/	-10	-60	-50
RG to Hip	0.1	-40	-60	-40
RG to Knee	0.05	-40	-60	-40
RG to Ankle	0.02	-40	-60	-40
Hip to BFP	0.967	-40	-60	-40
Hip to RF	0.236	-40	-59	-40
Knee to BFP	0.365	-40	-59	-40
Knee to RF	0.872	-40	-60	-40
Knee to GA	1	-40	-60	-40
Ankle to GA	0.3	-40	-59	-40
PF to Ia	0.5	-40	-60	-55
Between Ia	0.5	-70	-60	-40
Ia to MN	2	-100	-60	-40
MN to RE	0.5	-40	-100	-10
Between R	0.5	-70	-60	-40
R to MN	0.5	-100	-60	-40

0.5

-70

Table 2. Synapse parameters.

PFs to MNs	g (μS)		
BFA	2		
IP	3		
BFP	6.4		
RF	5.8		
VA	5		
GA	4		
SO	8		
TA	2		

References

R to Ia

1. Bouman, A., et al.: Autonomous Spot: Long-Range Autonomous Exploration of Extreme Environments with Legged Locomotion (2020)

-40

-60

- Feng, S., Whitman, E., Xinjilefu, X., Atkeson, C.G.: Optimization based full body control for the atlas robot. In: Proceedings of the 2014 IEEE-RAS International Conference on Humanoid Robots, pp. 120–127. IEEE, Madrid, Spain, November 2014
- 3. Hubicki, C., et al.: ATRIAS: design and validation of a tether-free 3D-capable spring-mass bipedal robot. Int. J. Robot. Res. **35**, 1497–1521 (2016). https://doi.org/10.1177/027836491 6648388
- 4. Hutter, M., et al.: ANYmal a highly mobile and dynamic quadrupedal robot. In: Proceedings of the 2016 IEEE/RSJ International Conference on Intelligent Robots and Systems (IROS), pp. 38–44, October 2016
- Geng, T., Porr, B., Worgotter, F.: Self-stabilized biped walking under control of a novel reflexive network. In: Proceedings of the 2005 IEEE/RSJ International Conference on Intelligent Robots and Systems, pp. 3269–3274, August 2005

- Ijspeert, A.J., Crespi, A., Ryczko, D., Cabelguen, J.-M.: From swimming to walking with a salamander robot driven by a spinal cord model. Science 315, 1416–1420 (2007). https://doi. org/10.1126/science.1138353
- 7. Yang, W., Kim, H., You, B.J.: Biologically inspired self-stabilizing control for bipedal robots. Int. J. Adv. Rob. Syst. 10, 144 (2013). https://doi.org/10.5772/55463
- Szczecinski, N.S., et al.: Introducing MantisBot: hexapod robot controlled by a high-fidelity, real-time neural simulation. In: Proceedings of the 2015 IEEE/RSJ International Conference on Intelligent Robots and Systems (IROS), pp. 3875–3881. IEEE, Hamburg, Germany, September 2015
- Kimura, H., Fukuoka, Y., Cohen, A.H.: Adaptive dynamic walking of a quadruped robot on natural ground based on biological concepts. Int. J. Robot. Res. (2016).https://doi.org/10. 1177/0278364907078089
- Hunt, A., Szczecinski, N., Quinn, R.: Development and training of a neural controller for hind leg walking in a dog robot. Front. Neurorobot. 11 (2017). https://doi.org/10.3389/fnbot. 2017.00018
- Kim, J.-Y., Park, I.-W., Oh, J.-H.: Walking control algorithm of biped humanoid robot on uneven and inclined floor. J. Intell. Robot. Syst. 48, 457–484 (2007). https://doi.org/10.1007/ s10846-006-9107-8
- 12. Schilling, M., et al.: A hexapod walker using a heterarchical architecture for action selection. Front. Comput. Neurosci. 7, 126 (2013). https://doi.org/10.3389/fncom.2013.00126
- 13. Szczecinski, N.S., Brown, A.E., Bender, J.A., Quinn, R.D., Ritzmann, R.E.: A neurome-chanical simulation of insect walking and transition to turning of the cockroach Blaberus discoidalis. Biol. Cybern. **108**(1), 1–21 (2013). https://doi.org/10.1007/s00422-013-0573-3
- Hunt, A., Schmidt, M., Fischer, M., Quinn, R.: A biologically based neural system coordinates the joints and legs of a tetrapod. Bioinspiration Biomim. 10, 055004 (2015). https://doi.org/ 10.1088/1748-3190/10/5/055004
- 15. Deng, K., et al.: Neuromechanical model of rat hindlimb walking with two-layer CPGs. Biomimetics **4**, 21 (2019)
- Forssberg, H., Grillner, S., Halbertsma, J., Rossignol, S.: The locomotion of the low spinal cat II. Interlimb coordination. . Acta Physiol. Scand. 108, 283–295 (1980). https://doi.org/10. 1111/j.1748-1716.1980.tb06534.x
- Frigon, A., Hurteau, M.-F., Thibaudier, Y., Leblond, H., Telonio, A., D'Angelo, G.: Split-belt walking alters the relationship between locomotor phases and cycle duration across speeds in intact and chronic spinalized adult cats. J. Neurosci. 33, 8559–8566 (2013). https://doi.org/10.1523/JNEUROSCI.3931-12.2013
- Frigon, A., Thibaudier, Y., Hurteau, M.-F.: Modulation of forelimb and hindlimb muscle activity during quadrupedal tied-belt and split-belt locomotion in intact cats. Neuroscience 290, 266–278 (2015). https://doi.org/10.1016/j.neuroscience.2014.12.084
- Brown, T.: The Intrinsic Factors in the Act of Progression in the Mammal, Royal Society of London (1911)
- Grillner, S., McCLELLAN, A., Sigvardt, K., Wallén, P., Wilén, M.: Activation of NMDA-receptors elicits fictive locomotion in lamprey spinal cord in vitro. Acta Physiol. Scand. 113, 549–551 (1981). https://doi.org/10.1111/j.1748-1716.1981.tb06937.x
- Brown, T.G.: On the nature of the fundamental activity of the nervous centres; together with an
 analysis of the conditioning of rhythmic activity in progression, and a theory of the evolution
 of function in the nervous system. J. Physiol. 48, 18–46 (1914). https://doi.org/10.1113/jph
 ysiol.1914.sp001646
- Hägglund, M., Dougherty, K.J., Borgius, L., Itohara, S., Iwasato, T., Kiehn, O.: Optogenetic dissection reveals multiple rhythmogenic modules underlying locomotion. PNAS 110, 11589– 11594 (2013). https://doi.org/10.1073/pnas.1304365110

- Bässler, U., Büschges, A.: Pattern generation for stick insect walking movements—multisensory control of a locomotor program. Brain Res. Rev. 27, 65–88 (1998). https://doi.org/10.1016/S0165-0173(98)00006-X
- Arbas, E.A., Calabrese, R.L.: Ionic conductances underlying the activity of interneurons that control heartbeat in the medicinal leech. J. Neurosci. 7, 3945–3952 (1987). https://doi.org/ 10.1523/JNEUROSCI.07-12-03945.1987
- Tryba, A.K., Peña, F., Ramirez, J.-M.: Gasping activity in vitro: a rhythm dependent on 5-HT2A receptors. J. Neurosci. 26, 2623–2634 (2006). https://doi.org/10.1523/JNEUROSCI. 4186-05.2006
- 26. Grillner, S., Zangger, P.: On the central generation of locomotion in the low spinal cat. Exp. Brain Res. **34**, 241–261 (1979)
- Rybak, I.A., Shevtsova, N.A., Lafreniere-Roula, M., McCrea, D.A.: Modelling spinal circuitry involved in locomotor pattern generation: insights from deletions during fictive locomotion.
 J. Physiol. 577, 617–639 (2006). https://doi.org/10.1113/jphysiol.2006.118703
- Deng, K., Szczecinski, N.S., Hunt, A.J., Chiel, H.J., Quinn, R.D.: Kinematic and kinetic analysis of a biomechanical model of rat hind limb with biarticular muscles. In: Vouloutsi, V., Mura, A., Tauber, F., Speck, T., Prescott, T.J., Verschure, P.F.M.J. (eds.) Biomimetic and Biohybrid Systems. Living Machines 2020. LNCS, vol. 12413, pp. 55–67. Springer, Cham (2020). https://doi.org/10.1007/978-3-030-64313-3_7
- 29. Young, F., Rode, C., Hunt, A., Quinn, R.: Analyzing moment arm profiles in a full-muscle rat hindlimb model. Biomimetics 4, 10 (2019). https://doi.org/10.3390/biomimetics4010010
- Deng, K., et al.: Biomechanical and sensory feedback regularize the behavior of different locomotor central pattern generators. Biomimetics 7, 226 (2022). https://doi.org/10.3390/biomimetics7040226
- 31. Cofer, D., Cymbalyuk, G., Reid, J., Zhu, Y., Heitler, W.J., Edwards, D.H.: AnimatLab: a 3D graphics environment for neuromechanical simulations. J. Neurosci. Methods **187**, 280–288 (2010). https://doi.org/10.1016/j.jneumeth.2010.01.005
- Shadmehr, R., Arbib, M.A.: A mathematical analysis of the force-stiffness characteristics of muscles in control of a single joint system. Biol. Cybern. 66, 463–477 (1992). https://doi.org/ 10.1007/BF00204111
- 33. Shadmehr, R., Wise, S.: A Mathematical Muscle Model
- Szczecinski, N.S., Hunt, A.J., Quinn, R.D.: Design process and tools for dynamic neuromechanical models and robot controllers. Biol. Cybern. 111(1), 105–127 (2017). https://doi.org/ 10.1007/s00422-017-0711-4
- Szczecinski, N.S., Quinn, R.D., Hunt, A.J.: Extending the functional subnetwork approach to a generalized linear integrate-and-fire neuron model. Front. Neurorobot. 14 (2020). https://doi.org/10.3389/fnbot.2020.577804
- 36. Markin, S.N., Klishko, A.N., Shevtsova, N.A., Lemay, M.A., Prilutsky, B.I., Rybak, I.A.: Afferent control of locomotor CPG: insights from a simple neuromechanical model. Ann. N. Y. Acad. Sci. **1198**, 21–34 (2010). https://doi.org/10.1111/j.1749-6632.2010.05435.x
- Daun-Gruhn, S., Büschges, A.: From neuron to behavior: dynamic equation-based prediction of biological processes in motor control. Biol. Cybern. 105, 71–88 (2011). https://doi.org/10. 1007/s00422-011-0446-6

- 38. Markin, S., Klishko, A., Shevtsova, N., Lemay, M., Prilutsky, B., Rybak, I.: A neuromechanical model of spinal control of locomotion. In: Prilutsky, B., Edwards, D. (eds.) Neuromechanical Modeling of Posture and Locomotion, pp. 21–65. SSCN. Springer, New York, NY (2016). ISBN 978-1-4939-3267-2. https://doi.org/10.1007/978-1-4939-3267-2_2
- 39. Shevtsova, N., Hamade, K., Chakrabarty, S., Markin, S., Prilutsky, B., Rybak, I.: Modeling the organization of spinal cord neural circuits controlling two-joint muscles. In: Prilutsky, B., Edwards, D. (eds.) Neuromechanical Modeling of Posture and Locomotion, pp. 121–162. SSCN. Springer, New York, NY (2016). ISBN 978-1-4939-3267-2. https://doi.org/10.1007/978-1-4939-3267-2_5